ELSEVIER

PII: S0032-3861(96)00803-8

Polymer Vol. 38 No. 10, pp. 2379–2388, 1997

0032-3861/97/$17.00+0.00

Compressive properties of aramid fibres

M. C. Andrews, D. Lu and R. J. Young*
Manchester Materials Science Centre, UMIST/University of Manchester, Grosvenor Street, Manchester M1 7HS, UK
(Received 20 July 1995; revised 8 August 1996)

A four-point bending beam method has been employed in order to study the compressive properties of a number of well-characterized aromatic polyamide (aramid) fibres using a combination of Raman spectroscopy and optical microscopy. Raman spectroscopy has been used to follow the molecular deformation of the aramid fibres in both tension and compression, from which the stress/strain data have been derived. The Raman technique has also been used to map the variation of stress along aramid fibres in compression in order to define the regions of localized compressive failure indicated by the formation of visible kink bands. Using a combination of Raman spectroscopy and optical microscopy it is found that the compressive kink band failure occurs through a process of yielding of the highly-oriented fibres in compression. The values of initial compressive failure strain are found to depend upon the orientation parameter of the molecules in the fibres and agree well with those predicted by a modified series model for fibre yielding. Possible methods of improving the compressive behaviour of aramid fibres are discussed. © 1997 Elsevier Science Ltd.

(Keywords: aramid fibres; compression properties; Raman spectroscopy)

INTRODUCTION

The spinning of fibres from liquid crystalline solutions[1,2] has enabled fibres such as aromatic polyamides (aramids) to be produced with a high degree of molecular alignment. Such fibres have tensile strengths of 2–3 GPa and Young's moduli of up to 165 GPa[3]. In comparison to their tensile behaviour however, the compressive properties of these fibres are less impressive[4–14].

Several test methods such as the elastica loop test[15], the tensile recoil test[6], the single-fibre composite technique[9], the micro tensile/compression method[10] and the cantilever beam method[11] have been developed and employed in order to measure the compressive properties of fibres. These methods have been reviewed recently by Kozey *et al.*[16] and in the case of aramids have been found to give different values of compressive strength. In order to determine the compressive strength of a fibre the compressive modulus is often assumed to be equal to the tensile modulus, an assumption that has been shown recently to be inappropriate[13].

The compressive behaviour of high-performance fibres has been shown by some workers[7] to be dependent upon the tensile modulus of the fibres, and by other workers[6,14] to be independent of the tensile properties but dependent upon molecular interactions. Therefore one of the main difficulties in the study of compressive properties of polymer fibres is the lack of accurate and reproducible experimental data due to the small diameter of the fibres and the different test methods employed. These findings make the modelling of the compressive behaviour difficult.

Raman spectroscopy has been used successfully to study the deformation behaviour of high performance aramid fibres[3,17,18]. For such fibres certain Raman bands have been found to be sensitive to the applied stress[3,17,18] and shift generally to lower frequencies under tension and to higher frequencies upon compression[12,13]. The Raman-active band shifts reflect the deformation of polymer backbone bonds in response to the applied stress[3]. The Raman technique is therefore a direct method of studying the deformation at the molecular level.

The Raman technique has been employed recently to study the compressive properties of liquid crystalline polymer fibres[12,13] using a cantilever beam method[11]. The stress-induced Raman shifts have been used to monitor closely the stress along a fibre in both tension and compression. A disadvantage of the cantilever beam method however, is that the stress is determined at different points along the length of the fibre. This may give rise to statistical variations due to local stress concentrations given that the fibre is unlikely to be represented by a uniform cylinder with uniform properties. Also the formation of kink bands due to localized compressive failure may give rise to a non-uniform stress distribution along the fibre that cannot be totally distinguished from the distribution of stress due to the deflection of the beam.

In this present study the compressive deformation of aramid fibres has been investigated using both optical and Raman microscopy on a set of well-characterized fibres[3] processed in such a way as to produce a systematic variation in their structure. The Raman technique has been employed in order to determine the compressive properties of the aramid fibres deformed using a four-point bending beam method. The advantage of this test method is that the stress and strain are uniform between the loading points. This enables the compressive stress to be determined at any point along a fibre and also allows

* To whom correspondence should be addressed

the variation of stress due to localized compressive failure to be determined along the fibre. It will also be shown that the values of compressive failure strain for the well-oriented aramid fibres agree well with the values of compressive failure strain predicted by a modified series model[19]. This indicates that the compressive failure of the aramid fibres is determined by the sequential plastic deformation of the polymer chains during yielding.

EXPERIMENTAL

Fibres

Experimental and commercial poly(*p*-phenylene terephthalamide) aramid fibres, supplied by E.I. Du Pont de Nemours, Wilmington, U.S.A., and Akzo Nobel, Arnhem, The Netherlands, were used in this study. Details of their mechanical properties are given in *Table 1*. A, B and C fibres are three different groups of experimental fibres that were prepared with systematic changes in processing conditions in order to produce fibres with a variety of mechanical properties and different skin/core structures. Commercial Kevlar-type fibres (Kevlar 29, Kevlar 49 and Kevlar 149) two of which (Kevlar 49 and Kevlar 149) had been heat treated, and Twaron LM and Twaron HM fibres are also presented for comparison. The structures and mechanical properties of these fibres have been investigated and presented in earlier publications[3,18,20].

Specimen preparation

The tensile properties of the aramid fibres used in this study have been determined previously[3,20]. For tensile Raman deformation studies, individual fibres were mounted on a small aluminium straining rig fitted with a micrometre enabling the fibres with a gauge length of 20 mm to be extended in small steps of the order of 10 μm, giving a precision of measuring strain of $\pm 0.05\%$.

In order to study the compressive properties, the aramid fibres were placed on the surface of rectangular poly(methyl methacrylate) (PMMA) beams. A thin film was then cast from a PMMA/chloroform solution over the fibre on the surface of the beam. A strain gauge was bonded to the surface of the beam, in the centre, next to the aramid fibre. The samples were deformed using a four-point bending rig with the fibre positioned on the compressive surface of the beam, as shown schematically in *Figure 1*.

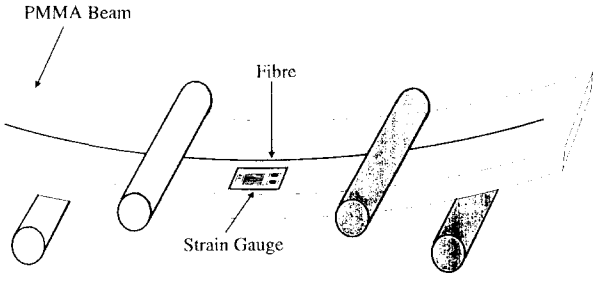

Figure 1 Schematic diagram of the four-point bending arrangement used for deforming the aramid fibres in compression

Optical microscopy

The bending rig was placed onto the stage of an Olympus optical microscope operated in the transmission mode. A $\times 20$ long-working-distance objective lens and a $\times 2.5$ eye piece were employed to give a total magnification of $\times 50$. The fibres were compressed using a strain step of -0.034%. The number of kink bands was counted visually *in situ* after each deformation step. Optical micrographs were also obtained at -0.25% strain intervals. The compressive failure strain, e_c^*, was taken as the strain at which kink bands could be observed visually. Three measurements were made for each fibre sample and a mean value was calculated.

Raman spectroscopy

The specimens were placed on the stage of a modified Olympus BH-2 optical microscope connected via a set of collection optics to a Spex 1000 M single monochromator. The 632.8 mm red line of a 15 mW helium–neon laser, focused to a ~ 3 μm spot on the surface of the fibre, was employed as the excitation source. A highly-sensitive Wright Instruments charge-coupled device (CCD) camera, cooled with liquid nitrogen, was used to collect the Raman spectra using an exposure time of 7 s. The peak position of the 1610 cm^{-1} aramid Raman band was determined from Raman spectra obtained during the tensile deformation of individual aramid fibres in air as described elsewhere[3,17,18,20]. The peak position of the 1610 cm^{-1} aramid Raman band was also determined from Raman spectra recorded at one point along the aramid fibres in compression at increments of -0.034% compressive strain up to -1.4% and also along the length of the compressed aramid fibres, between the loading points, at different strain levels.

Table 1 Details of the tensile properties of the different aramid fibres

Fibre	Diameter (μm)	Tensile modulus (GPa)	Fracture stress (GPa)	Fracture strain (%)	Tension $d\Delta\nu/de$ ($cm^{-1}/\%$)
A1	10.3	128	2.7	2.2	-4.0 ± 0.2
A7	10.2	94	1.8	1.8	-4.0 ± 0.3
B1	15.8	116	2.2	2.1	-3.9 ± 0.2
B7	14.0	90	2.0	2.4	-3.6 ± 0.1
C1	18.7	99	2.7	2.9	-3.3 ± 0.1
C7	19.1	67	2.1	3.0	-2.1 ± 0.1
Twaron LM	12.5	76	3.4	3.5	-3.1 ± 0.3
Twaron HM	11.8	105	2.8	2.4	-3.8 ± 0.3
Kevlar 29	12.8	94	2.5	2.5	-3.2 ± 0.2
Kevlar 49	12.5	124	2.3	1.8	-4.0 ± 0.1
Kevlar 149	12.4	161	1.7	1.0	-5.2 ± 0.4

RESULTS AND DISCUSSION

Raman spectroscopy

Single-fibre deformation. *Figure 2* shows the position of the 1610 cm^{-1} aramid Raman band for a single Kevlar 49 fibre undeformed, at +0.5% tensile strain and −0.5% compressive strain. It can be seen that there is a shift of the band to lower frequency in tension as reported earlier[3,17,18], and a shift to higher frequency in compression[12,13]. This enables the Raman technique to be employed for following fibre deformation.

Figure 3 shows the variation of the peak position of the 1610 cm^{-1} aramid Raman band with fibre strain for the Twaron LM, Twaron HM and Kevlar 49 fibres deformed in both tension and compression. The fibres were deformed in compression up to −1.4% strain and up to failure in tension. The solid lines are fits of the experimental data to a cubic spline function[21]. The variation of the peak position with fibre strain is approximately linear when the fibres are in tension. It can be seen that the slopes of the lines increase with increasing fibre tensile modulus (given in *Table 1*). In compression the peak position of the 1610 cm^{-1} Raman band shifts to higher frequency with increasing fibre strain reaching a maximum value where $e_f \sim -0.5\%$. In the case of the Twaron LM fibre the peak of the Raman band is approximately constant when the compressive fibre strain exceeds −0.5%. For the Twaron HM and the Kevlar 49 fibres the peak position of the 1610 cm^{-1} aramid Raman band reaches a maximum value of ~1612.75 cm^{-1} between −0.5% and −0.6% and then decreases slightly reaching an approximately constant plateau value. It is clearly shown that the shift of the 1610 cm^{-1} Raman band is considerably greater in tension than it is in compression.

It has been shown for a large number of aramid fibres, regardless of structure, that the shift of the 1610 cm^{-1} aramid Raman band is proportional to stress[3,13,18] and the rate of shift of the Raman band with stress is equal to ~4.0 cm^{-1} GPa^{-1}. Using this value it is possible to derive the stress/strain curves for the aramid fibres, shown in *Figure 4*, from the Raman data shown in *Figure 3*. For each of the aramid fibres tested in compression the maximum compressive stress is less than 500 MPa which is considerably less than the tensile strength of the fibres. The compressive strength of the Twaron HM and Kevlar 49 fibres appears to be slightly higher than the compressive strength of the lower modulus Twaron LM fibre although the difference is relatively small. Another point to note is that the slope of the stress/strain curves decreases with increasing compressive strain indicating a reduction in the compressive modulus of the fibre. Therefore in order to calculate the compressive strength of the aramid fibres the compressive modulus should not be assumed to be equal to the tensile modulus of the fibres.

It is important to note the continuous change in slope between the tension and compression region corresponding to a continuous change in fibre modulus. Vlattas and Galiotis[12] fitted similar data to two straight lines with slightly different slopes. However, there cannot be a sudden change in modulus through the origin and molecular mechanics requires that such a change can only be continuous as shown in *Figure 4*. In a subsequent paper[13] they modified their plots to give a continually varying slope consistent with our own findings, as shown in *Figure 4*.

In a recent paper by Kawabata *et al.*[22] the compressive properties of several high-performance fibres, including aramids, were determined from the compressive properties of micro-composite rods, ~1 mm in diameter with a fibre volume fraction of 80–85%. Their compressive stress/strain data for Kevlar 29, 49 and 149 aramid fibres, derived from the deformation of the aramid rods, are remarkably similar to the data obtained from the

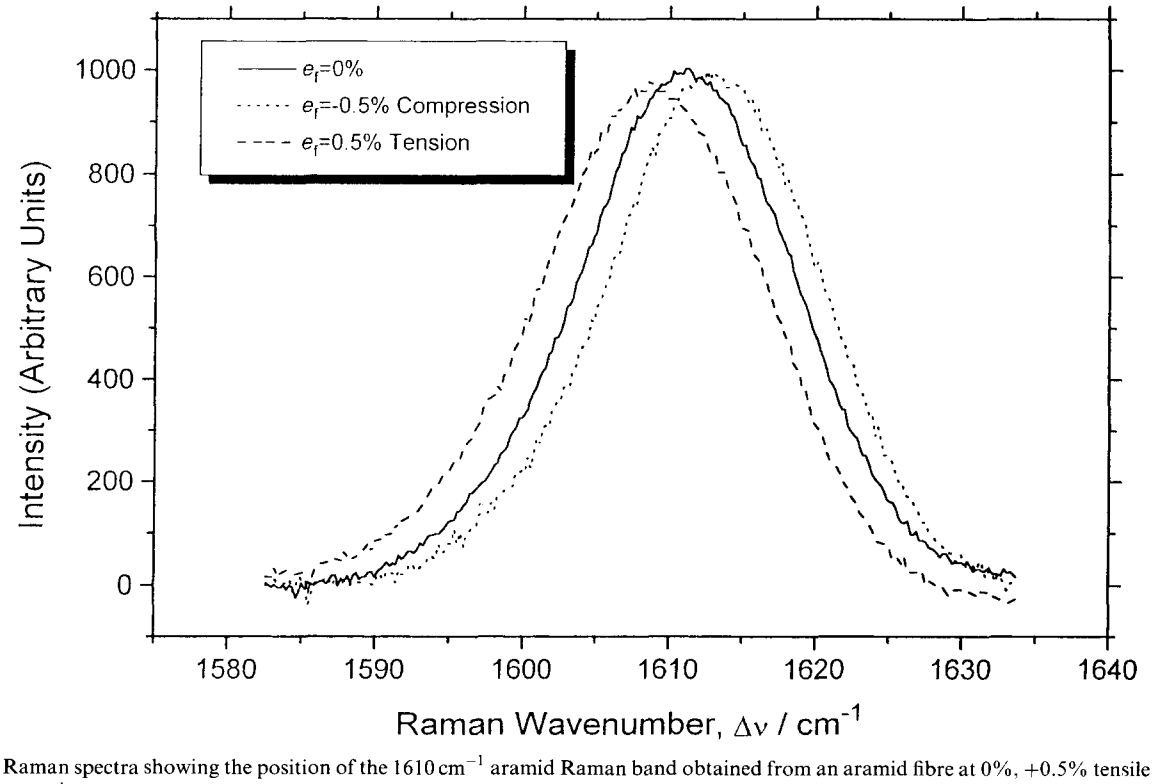

Figure 2 Raman spectra showing the position of the 1610 cm^{-1} aramid Raman band obtained from an aramid fibre at 0%, +0.5% tensile and −0.5% compressive strain

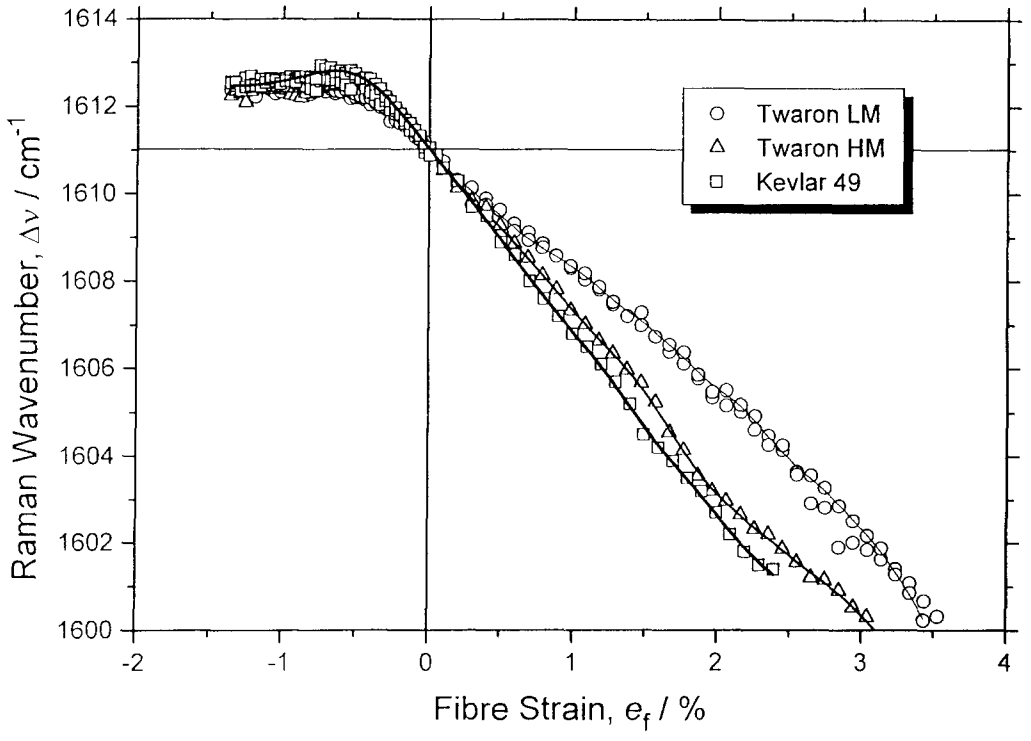

Figure 3 Variation of the peak position of the 1610 cm^{-1} aramid Raman band with fibre strain for three different aramid fibres deformed in both tension and compression

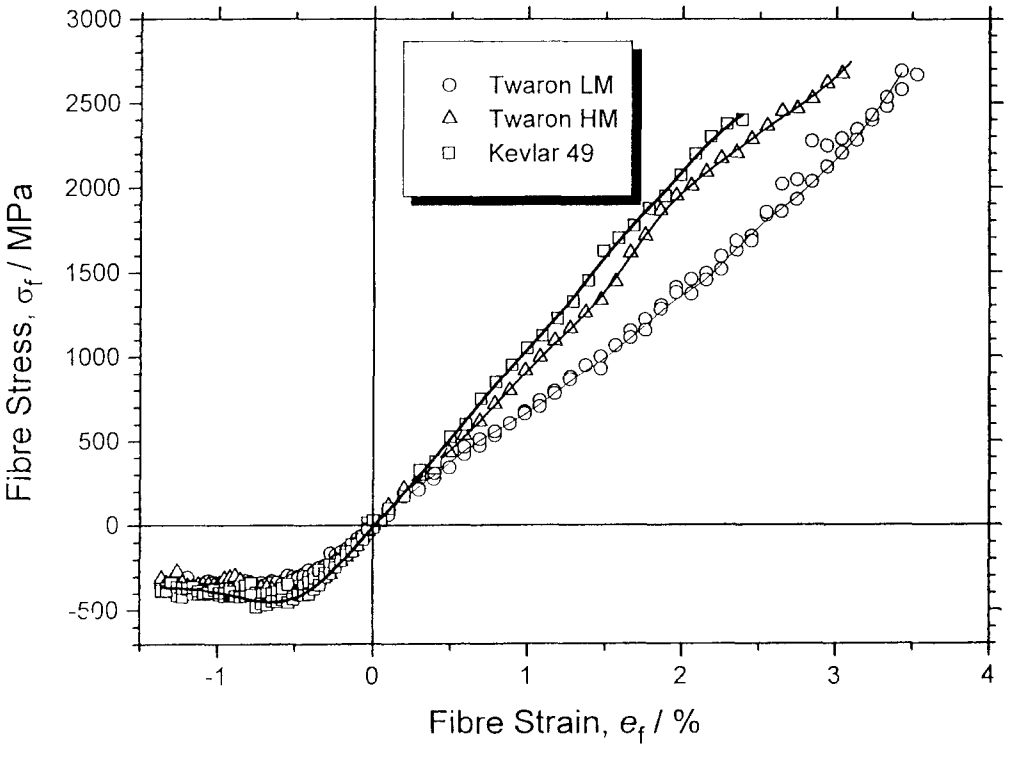

Figure 4 Derived variation of fibre stress with fibre strain for three different aramid fibres deformed in both tension and compression

deformation of the individual fibres shown in *Figure 4*. However, the values of compressive strength are slightly lower for the fibres in the micro-composite rods (~300 MPa) compared with the deformation of the individual aramid fibres (~400 MPa). This may be a result of cooperative compressive failure through kink band propagation between adjacent fibres in the rods[22] reducing the composite compressive failure stress.

Fibre strain mapping. In order to observe the effect of local stress concentrations due to compressive failure and kink band formation the peak position of the 1610 cm^{-1} aramid Raman band has been determined from Raman spectra taken from different positions along Kevlar 49 fibres in compression. *Figure 5* shows the statistical distribution of the 1610 cm^{-1} peak position taken from over 50 measurements along the length of a Kevlar

49 fibre at different compressive strains. The distribution of peak position shifts to higher frequency with increasing compressive strain and also broadens indicated by the fact that the standard deviation increases from 0.11 cm^{-1} where $e_f = 0\%$ to 0.16 cm^{-1} where $e_f = -1.2\%$. At high compressive strains it is found that the statistical distribution is dependent upon whether or not the laser was focused on a kink band. This is demonstrated in *Figure 6*, which shows the peak position of the 1610 cm^{-1} aramid Raman band determined from Raman spectra recorded at 50 points along a Kevlar 49 fibre where the laser was focused either between kink bands or on a kink band. It is evident that the mean position of the 1610 cm^{-1} Raman band is ~0.2 cm^{-1} lower for measurements taken where the laser was focused on a kink band and therefore indicates a difference in local stress.

The effect of localized compressive failure along a Kevlar 49 fibre is demonstrated in *Figure 7* which shows the peak position of the 1610 cm^{-1} Raman band determined from spectra recorded at 5 μm intervals along a 300 μm section of a Kevlar 49 fibre. Similar data have also been obtained for other aramid fibres. The schematic diagram represents the positions of kink bands along the short 300 μm section of the fibre. From the values of Raman band peak position, shown in *Figure 7*, there appears to be a distribution of fibre stress along the region between the individual kink bands. The process of kink band formation may be considered to be equivalent to a fragmentation process[23] in compression. Fragmentation tests are normally undertaken for model single-fibre composites deformed in tension whereby fibre fracture occurs randomly as the overall stress is increased[23]. It has been found using Raman spectroscopy that there is a distribution of stress in the broken fragments. It is zero at the broken ends and then, if there is good bonding, increases along the fibre until it saturates at a plateau value along the central region of the fragment with stress transfer from the matrix to the fibre taking place through a shear–lag process[23]. It appears likely that the kink bands may be acting as compressive

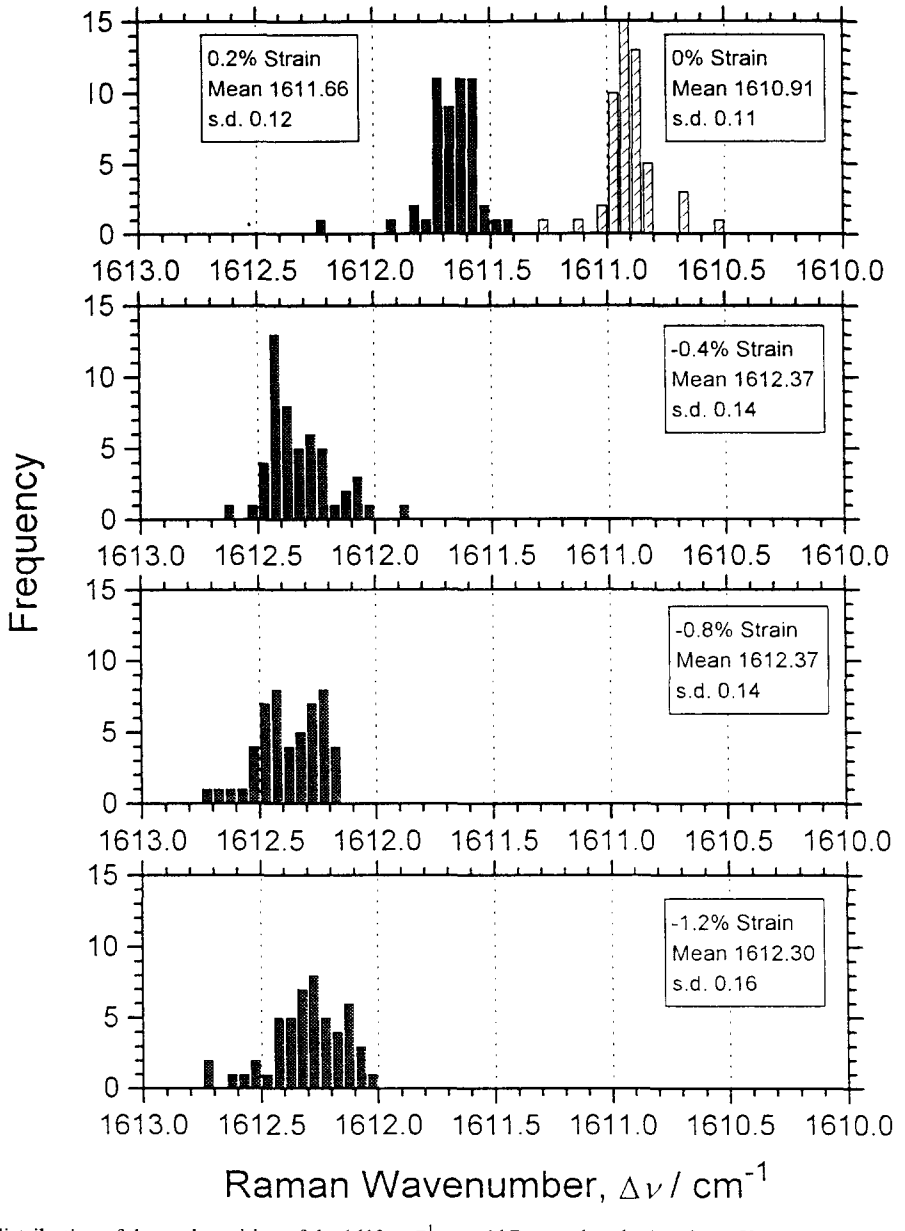

Figure 5 Statistical distribution of the peak position of the 1610 cm^{-1} aramid Raman band taken from 50 measurements along a Kevlar 49 fibre in the undeformed state and at different levels of compressive strain

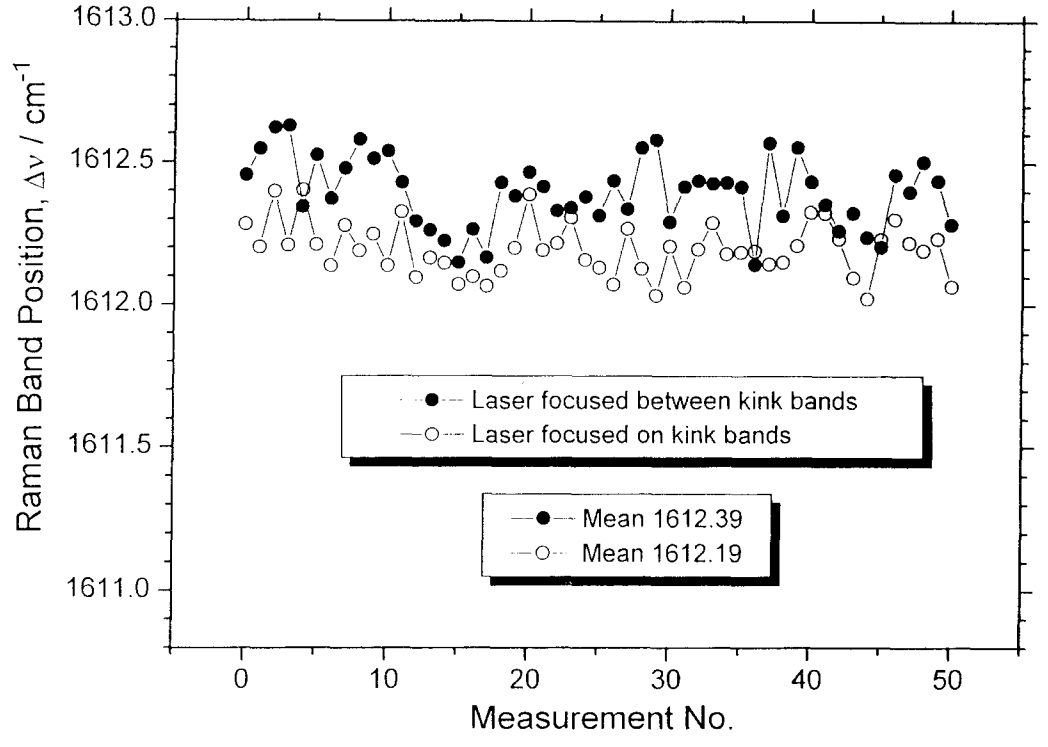

Figure 6 Peak position of the 1610 cm^{-1} aramid Raman band recorded at 50 points along a compressed Kevlar 49 fibre, $e_f = 0.8\%$, by focusing the laser either on a kink band or between kink bands

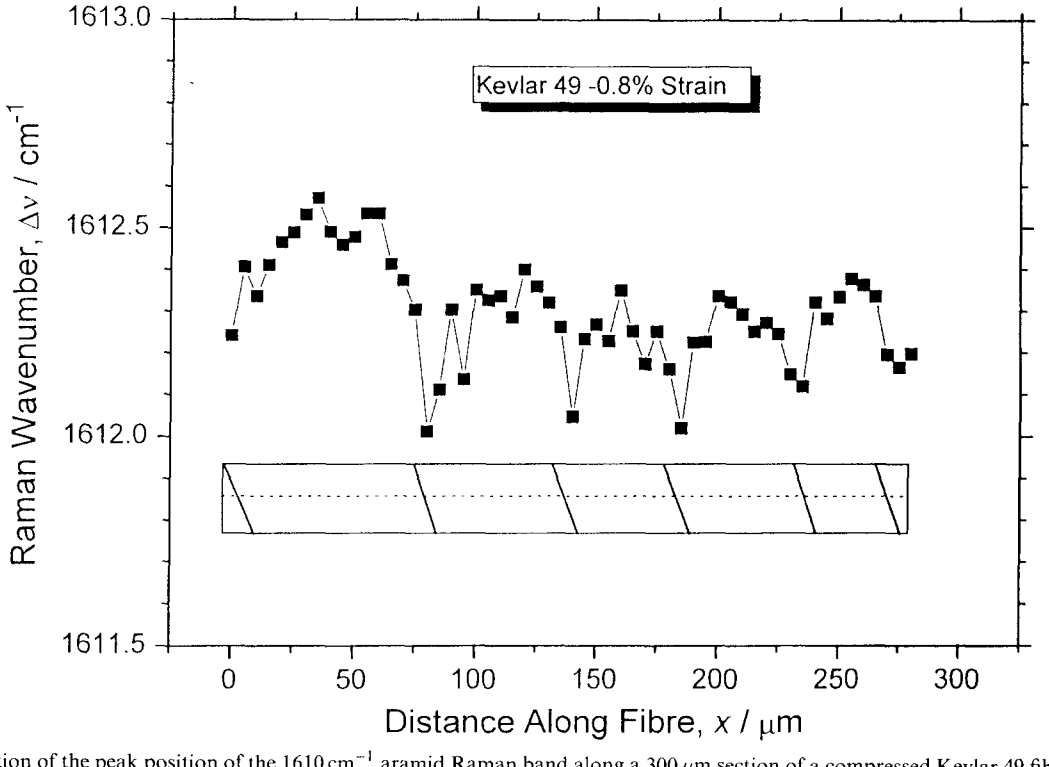

Figure 7 Variation of the peak position of the 1610 cm^{-1} aramid Raman band along a 300 μm section of a compressed Kevlar 49 fibre, $e_f = -0.8\%$. The schematic diagram shows the positions of kink bands and also the positions where the Raman spectra were recorded along the fibre

'cracks' over which little or no stress is transferred and that stress transfer between the kink bands may be taking place through a similar shear lag process. Wood *et al.*[24] have investigated the compressive failure of high modulus carbon fibres in model epoxy composites using the Raman technique and interpreted the failure as a similar fragmentation process.

As the compressive strain is increased further, more kink bands are formed that relieve the axial stress in the fibre. Therefore in this case the maximum stress never exceeds ~450 MPa, as shown in *Figure 4*. This process continues until the distance between kink bands becomes so short that the fibre stress cannot increase to cause further compressive failure and so the process reaches a

saturation point. The Raman technique can be used to define the effect of kink band formation upon the stress along the fibre, even though the kink bands are only ~0.5 μm wide and the laser beam is focused to a spot ~3 μm in diameter. This is demonstrated in *Figures 8* and *9* where the peak position of the 1610 cm^{-1} aramid Raman band (*Figure 8*) and the fibre stress (*Figure 9*) have been determined at 2.5 μm intervals along a Kevlar 49 fibre where two kink bands have formed. It is shown clearly that the stress is ~80 MPa lower at the position of the kink band. It is also extremely interesting to note that the small rise in stress between the two kink bands can be resolved. The findings described above therefore show clearly that the Raman technique is an extremely powerful technique of determining the variations in local stress along an aramid fibre deformed in compression.

Optical microscopy

Compressive failure of the aramid fibres is characterized by the formation of kink bands along the fibres. This can be seen from the optical micrographs in *Figure 10* which show a Kevlar 49 fibre at different levels of compressive strain. *Figure 11* shows the kink band density (number of kink bands per mm) along the Kevlar 49 fibre shown in *Figure 10* with increasing compressive strain. The peak position of the 1610 cm^{-1} aramid Raman band obtained from a Kevlar 49 fibre at different levels of compressive strain (*Figure 3*) is also shown in *Figure 11*. It is apparent that the first kink bands are observed where $0.3\% < e_f < 0.4\%$ and this occurs well before the wavenumber (or compressive stress) reaches a maximum. The lower curve, however, starts to deviate from linearity at about the same value of strain at which the kink bands are first observed. This behaviour is analogous to that of glassy polymers in which the yield process takes place through strain softening and the formation of shear bands which are first seen to occur at the point where the compressive stress/strain curve deviates from linearity[25] and not at the maximum stress. It is clear, therefore, that the initial observation of kink bands corresponds to the compressive failure strain e_c^*, of the aramid fibre. The

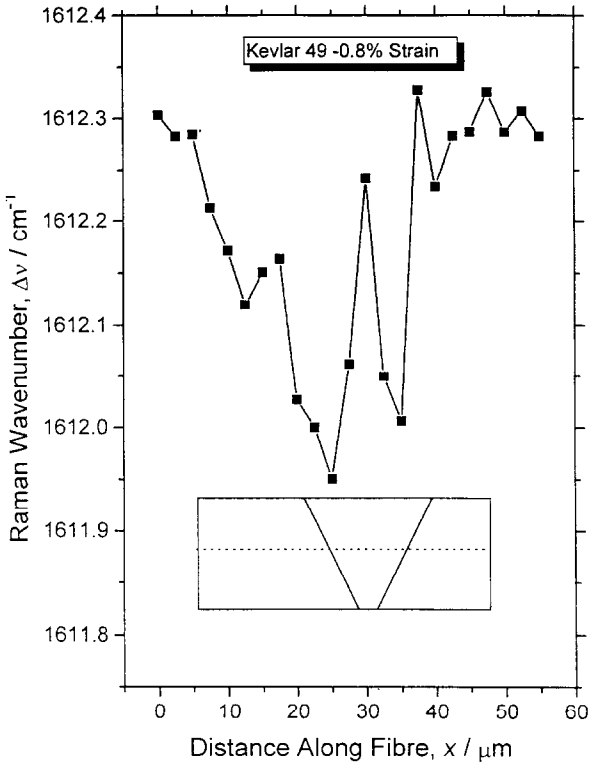

Figure 8 Variation of the peak position of the 1610 cm^{-1} aramid Raman band along a short 50 μm section of a compressed Kevlar 49 fibre, $e_f = -0.8\%$. The schematic diagram shows the positions of kink bands and also the positions where the Raman spectra were recorded along the fibre

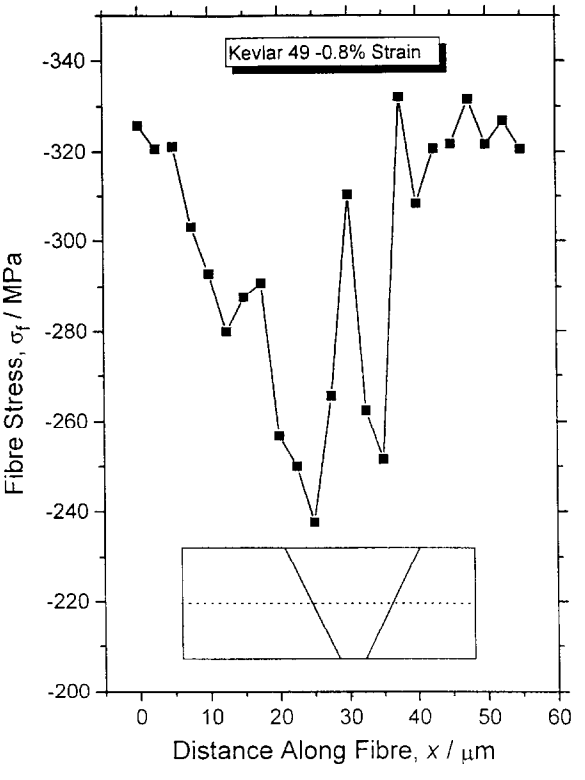

Figure 9 Derived variation of the fibre stress along a short 50 μm section of a compressed Kevlar 49 fibre, $e_f = -0.8\%$. The schematic diagram shows the positions of kink bands and also the positions where the Raman spectra were recorded along the fibre

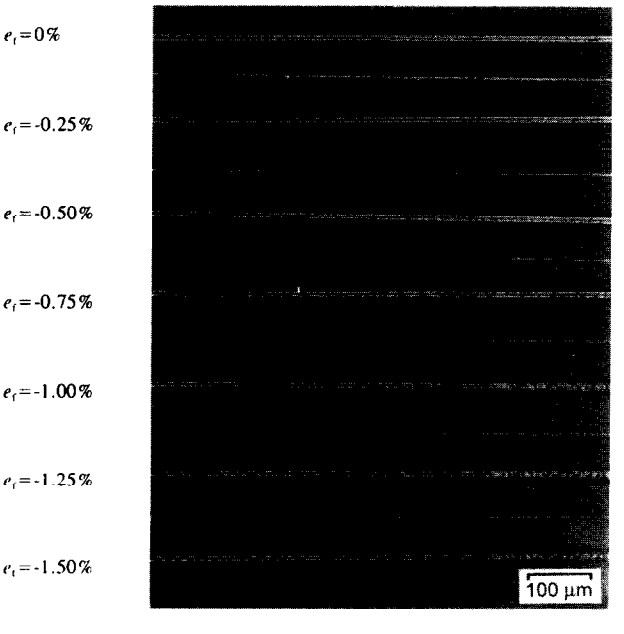

Figure 10 Optical micrographs of a Kevlar 49 fibre at different levels of compressive strain

compressive failure strain has been obtained using this visual observation method for several of the aramid fibres used in this study. The results are presented in *Table 2*.

It should be noted that Vlattas and Galiotis[13] claim that the failure criterion of aramid fibres is the point at which the lower curve in *Figure 11* reaches a maximum. They now assume that the change in slope of the curve is due to an inherent strain-softening of the molecules in compression rather than the onset of compressive failure as they assumed in their earlier paper[12]. The direct observations in *Figure 11* show clearly that the strain-softening is principally a result of kink band formation. Theoretical calculations of the compressive

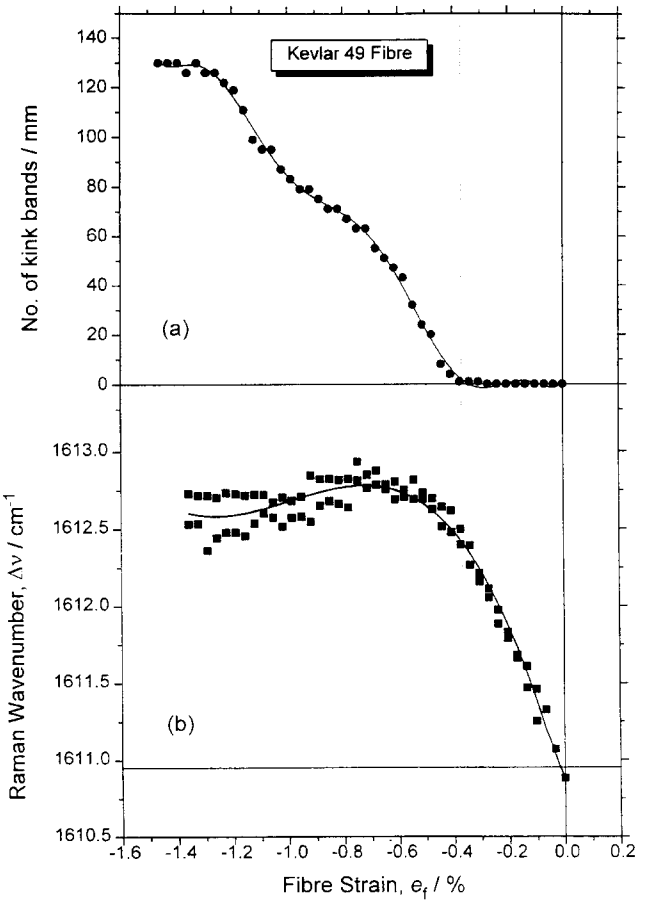

Figure 11 Variation of (a) kink band density (number of kink bands per mm) and (b) peak position of the 1610 cm^{-1} aramid Raman band with increasing compressive strain for a Kevlar 49 fibre

Table 2 Compressive properties of the aramid fibres obtained using optical microscopy and values of orientation parameter for fibre skin and core[3]

Fibre	Compressive failure strain, e_c^* (%)	$\langle \sin^2 \phi \rangle$	
		Skin	Core
A1	0.28 ± 0.04	0.0212	0.0301
A7	0.35 ± 0.01	0.0255	0.0489
B1	0.34 ± 0.01	0.0305	0.0355
B7	0.35 ± 0.01	0.0243	0.0473
C1	0.36 ± 0.09	0.0263	0.0271
C7	0.46 ± 0.01	0.0441	0.0529
Kevlar 29	0.37 ± 0.01	0.0235	0.0263
Kevlar 49	0.32 ± 0.08	0.0212	0.0251
Kevlar 149	0.30 ± 0.03	0.0209	0.0216

behaviour of rigid rod polymer[26] fibres have shown that significant strain softening occurs only at compressive strains in excess of 2%, which is nearly an order of magnitude in excess of the strain required for kink band formation.

Compressive failure mechanisms

The initiation of compressive failure corresponds to the position where the variation of the Raman band position with compressive fibre strain becomes approximately non-linear and indicates that the initiation of compressive failure of the aramid fibres by kink band formation occurs prior to the maximum value of compressive strength. This type of compressive failure has also been observed in aramid fibre-reinforced rods[22] deformed in compression and indicates the onset of yielding of the chain molecules, or individual filaments in the case of the rods. This is enhanced by the weak cohesive forces between the highly-oriented polymer molecules.

The yielding of polymer molecules in oriented polymer fibres has recently been related to the sequential plastic orientation process of polymer chains brought about by the resolved shear stress[19,27]. A modified series model has been developed to account for the shear stresses in the fibre which bring about rotation of the chains[19,27] in a fibril consisting of a series of rectangular domains of chains arranged end-to-end making angles ϕ to the fibre axis. It is predicted that the yield strain, e_y, in both tension and compression is given approximately by

$$e_y \approx \left(\frac{1}{E_c} + \frac{\langle \sin^2 \phi \rangle_E}{2g} \right) \frac{\tau_y}{\sin \phi_a \cos \phi_a} \quad (1)$$

where E_c is the chain modulus, $\langle \sin^2 \phi \rangle_E$ is the strain orientation parameter[3,27], g is the shear modulus and τ_y is the shear yield stress of the fibre above which plastic rotation of the chains can occur. The angles $\pm\phi_a$ are the orientation angles of an equivalent zig-zag bundle of aligned parallel chains in a fibre such that $\sin^2 \phi_a = \langle \sin^2 \phi \rangle_E$[27]. It should be noted that equation (1) is only an approximation since the detailed course of yielding in a real fibre will be controlled by the distribution of ϕ. It is envisaged[19] that plastic deformation will be initiated in crystalline domains at 45° to the compression axis which will be in the tail of the distribution of ϕ. In order to take into account the distribution in ϕ equation (1) can be approximated to[27,28]

$$e_y \approx \left(\frac{1}{E_c} + \frac{\langle \sin^2 \phi \rangle_E}{2g} \right) \frac{fg}{\sqrt{\langle \sin^2 \phi \rangle_E} \sqrt{1 - \langle \sin^2 \phi \rangle_E}} \quad (2)$$

assuming that τ_y is equal to a small but constant fraction, f, of the shear modulus, g, where $\tau_y = fg$. It should also be noted that equation (2) is only valid for values of $\langle \sin^2 \phi \rangle_E$ greater than zero since the yield mechanism envisaged could not occur for a perfectly-oriented fibre.

Figure 12a shows the values of compressive failure strain, e_c^*, plotted against the fibre core values of $\langle \sin^2 \phi \rangle_E$ given in *Table 2* determined experimentally from transmission electron microscopy. The lines have been calculated from equation (2) assuming that $e_c^* = e_y$, using values of $g = 1.5$ GPa and $E_c = 220$ GPa[19] and three different values of f (0.020, 0.025 and 0.03). These values of f are close to the values of f, $0.03 < f < 0.04$[19], determined experimentally from the measured tensile yield stress of isotropic aramid films for which $e_y = f/2$.

Although the range of values of $\langle \sin^2 \phi \rangle_E$ employed is not sufficiently large to provide a critical test of the theory it can be seen that the agreement between the experimental data and the theoretical curves is quite good. One important point to note is the rapid rise in failure strain predicted by the theory as $\langle \sin^2 \phi \rangle_E \rightarrow 0$. Unfortunately fibres with such high degrees of orientation were not available to test this prediction.

The theory can be examined further by rearranging equation (2) to give

$$e_y \sqrt{\langle \sin^2 \phi \rangle_E} \sqrt{1 - \langle \sin^2 \phi \rangle_E} \approx \frac{fg}{E_c} + \frac{f \langle \sin^2 \phi \rangle_E}{2} \quad (3)$$

The data from *Figure 12a* have been plotted in *Figure 12b* in accordance with equation (3). The straight line is a least squares fit to the data points and the slope of the line of 0.014 yields a value of the parameter f of 0.028, again similar to that determined elsewhere[19]. This value of f and the intercept on the y-axis give a value for the ratio E_c/g of about 195. If the crystal modulus E_c is assumed to be around 220 GPa then this ratio predicts a value of 1.15 GPa for the shear modulus, g, which is again similar to that used elsewhere[19].

The results of the analysis described above show clearly that the compressive failure of aramid fibres is determined by yielding involving the shear of polymer molecules past each other and is controlled by the initial orientation distribution of the molecular chains in the fibres.

Improvement of compressive properties of aramid fibres

It is worth considering at this stage if it is possible to improve the compressive behaviour of aramid fibres. It

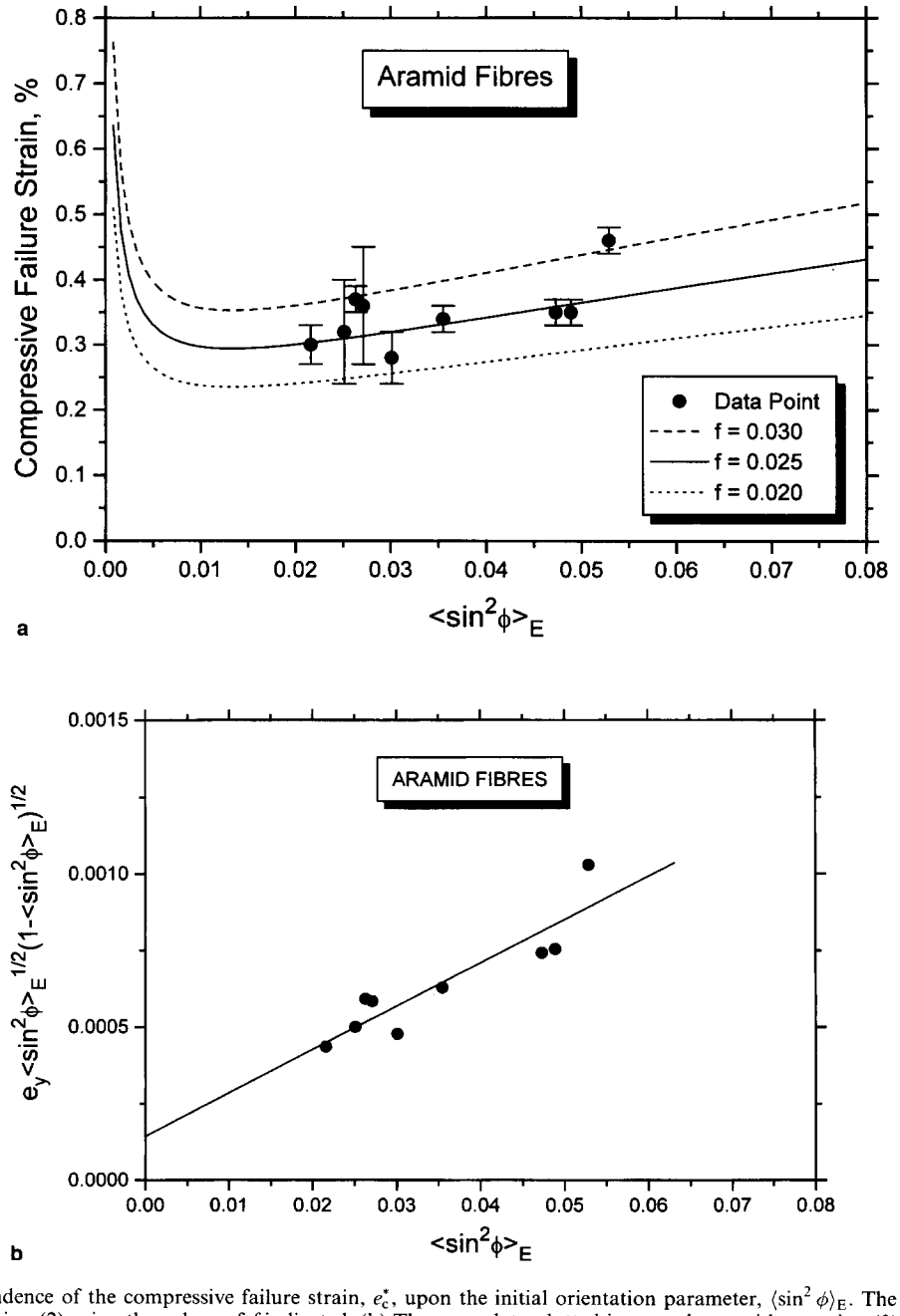

Figure 12 (a) Dependence of the compressive failure strain, e_c^*, upon the initial orientation parameter, $\langle \sin^2 \phi \rangle_E$. The theoretical lines have been calculated from equation (2) using the values of f indicated. (b) The same data plotted in accordance with equation (3). The straight line is a least squares fit of the data points

can be seen from *Figure 12* that the compressive failure strain increases with increasing $\langle \sin^2 \phi \rangle_E$ but the dependence is not strong. Hence producing fibres with higher values of $\langle \sin^2 \phi \rangle_E$ will not lead to dramatic improvements in compressive strength and moreover reducing the level of molecular orientation will lead to a significant deterioration in tensile properties. There is a rapid rise in failure strain at very low values of $\langle \sin^2 \phi \rangle_E$, i.e. for very highly-oriented fibres. It is unlikely, however, that improving the level of orientation, if that were possible, would significantly improve compressive properties. Experience with polydiacetylene single crystal fibres which have essentially perfect molecular alignment ($\langle \sin^2 \phi \rangle_E \sim 0$) has shown that they fail at relatively low strains in compression by a crystallographic twinning mechanism[29].

Inspection of equation (2) shows that one important parameter that controls the compressive strength of the fibres is the value of the shear modulus, g. This is relatively low for high-modulus fibres due to the weak secondary interchain bonding and is an important factor in leading to poor compressive properties. It may be possible to increase the value of this parameter by techniques such as crosslinking but such modifications again tend to damage the tensile properties.

There is a recent report by Harmer and Phillips[30] of the preparation of microcomposite fibres composed of an aramid polymer reinforced with SiC whiskers. They demonstrated that the fibres are more resistant to failure by kink band formation and that compressive strength of the fibres, as determined by the tensile recoil method[6], is improved significantly by a factor of at least two. It is thought that the SiC whiskers reinforce the fibres by making them resistant to the bending necessary for kink band formation.

CONCLUSIONS

It has been shown that Raman spectroscopy is an extremely powerful technique for following the molecular deformation of aramid fibres in compression as well as in tension. Using a four-point bending beam method to deform the fibres it is found that the compressive strength of the aramid fibres is considerably lower than the tensile strength of the fibres.

Raman spectroscopy has been employed successfully to monitor the distribution of fibre stress along aramid fibres in compression. It is shown that there is a non-uniform stress distribution along the fibre due to localized compression failure. Compressive failure of the aramid fibres is characterized by the formation of visible kink bands. The kink bands are found to relieve the overall axial stress on the fibre.

Compressive failure is initiated where the compressive stress/strain curve deviates from approximate linearity and indicates the onset of molecular yielding. This type of behaviour has also been observed in aramid fibre-reinforced rods[22] and is analogous to the plastic deformation of glassy polymers that yield by the formation of shear bands in compression. Yielding of the polymer molecules has been related to the sequential plastic orientation process of polymer chains. It has been shown that the values of compressive failure, determined from the visible formation of kink bands, agree well with the values of compressive yield strain determined by a modified series model[19] that accounts for the plastic deformation of the highly-oriented polymer molecules.

ACKNOWLEDGEMENTS

Financial support for the research work reported in this paper was kindly provided by the Engineering and Physical Science Research Council. The authors are grateful to E.I. Du Pont de Nemours and Akzo Nobel Central Research for the supply of fibres and valuable discussions. One of the authors (R.J.Y.) is grateful to the Royal Society for support in the form of the Wolfson Research Professorship in Materials Science.

REFERENCES

1. Kwolek, S. L., US Patent Nos 3671542, 1972 and 3819587, 1974.
2. Bair, T. I. and Morgan, P. W., US Patent Nos 3673143, 1972 and 3817941, 1974.
3. Young, R. J., Lu, D., Day, R. J., Knoff, W. F. and Davies, H. A., *J. Mat. Sci.* 1992, **27**, 5431.
4. Greenwood, J. H. and Rose, P. G., *J. Mat. Sci.* 1974, **9**, 1809.
5. Deteresa, S. J., Allen, S. R., Farris, R. J. and Porter, R. S., *J. Mat. Sci.* 1984, **19**, 57.
6. Allen, S. R., *J. Mat. Sci.* 1987, **22**, 853.
7. Van der Zwaag, S. and Kampschoer, G., in *Integration of Fundamental Polymer Science and Technology* (Eds P. J. Lemstra and L. A. Kleintjens), Vol. 2, Elsevier Applied Science, London, 1988, p. 545.
8. Van der Zwaag, S., Picken, S. J. and Van Sluijs, C. P., in *Integration of Fundamental Polymer Science and Technology* (eds P. J. Lemstra and L. A. Kleintjes), Vol. 3, Elsevier Applied Science, London, 1989, p. 199.
9. Young, R. J. and Ang, P. P., *Polymer* 1992, **33**, 975.
10. Fawaz, S. A., Palazotto, A. N. and Wang, C. S., *Polymer* 1992, **33**, 100.
11. Deteresa, S. J., Porter, R. S. and Farris, R. J., *J. Mat. Sci.* 1988, **23**, 1886.
12. Vlattas, C. and Galiotis, C., *Polymer* 1991, **32**, 1788.
13. Vlattas, C. and Galiotis, C., *Polymer* 1994, **35**, 2335.
14. Kumar, S. and Helminiak, T. E., in *The Materials Science and Engineering of Rigid-Rod Polymers* (eds W. W. Adams, R. K. Eby and D. E. McLemore), Materials Research Society Symposium Proceedings, Pittsburgh, 1989, p. 1.
15. Sinclair, D., *J. Appl. Phys.* 1950, **21**, 380.
16. Kozey, V. V., Jiang, H., Mehta, V. R. and Kumar, S., *J. Mat. Res.* 1995, **10**, 1044.
17. Galiotis, C., Robinson, I. M., Young, R. J., Smith, B. J. E. and Batchelder, D. N., *Polym. Commun.* 1985, **26**, 354.
18. Van der Zwaag, S., Northolt, M. G., Young, R. J., Galiotis, C., Robinson, I. M. and Batchelder, D. N., *Polym. Commun.* 1987, **28**, 276.
19. Northolt, M. G., Baltussen, J. J. M. and Schaffers-Korf, B., *Polymer* 1995, **36**, 3485.
20. Andrews, M. C., Young, R. J. and Mahy, J., *Composite Interfaces* 1995, **2**, 433.
21. Reinsch, C. H., *Numer. Math.* 1967, **10**, 177.
22. Kawabata, S., Kotani, T. and Yamashita, Y., *J. Text. Inst.* 1995, **86**, 347.
23. Huang, Y. and Young, R. J., *Comp. Sci. Tech.* 1994, **52**, 505.
24. Wood, J. R., Huang, Y., Young, R. J. and Marom, G., *comp. Sci. Tech.* 1995, **55**, 223.
25. Bowden, P. B., in *Physics of Glassy Polymers* (ed. R. N. Haward), Applied Science, London, 1973, Chap. 5.
26. Wierschke, S. G., Shoemaker, J. R., Haaland, P. D., Pachter, R. and Adams, W. W., *Polymer* 1992, **16**, 3357.
27. Baltussen, J. J. M., Tensile Deformation of Polymer Fibres, Ph.D. thesis, Technical University of Delft, The Netherlands, 1996.
28. Northolt, M. G., Personal communication.
29. Young, R. J., in *Developments in Oriented Polymers—2* (ed. I. M. Ward), Applied Science, London, 1987, p. 1.
30. Harmer, M. A. and Phillips, B. R., *J. Mat. Sci. Lett.* 1994, **13**, 930.